Available online at www.sciencedirect.com

SciVerse ScienceDirect

Ceramics International 39 (2013) 2651–2664

CERAMICS INTERNATIONAL

www.elsevier.com/locate/ceramint

Physiological and elastic properties of highly porous hydroxyapatite potential for integrated eye implants: Effects of SIRC and L-929 cell lines

Biswanath Kundu[a,*], Dipayan Sanyal[b], Debabrata Basu[†]

[a]*Bioceramics and Coating Division, CSIR-Central Glass and Ceramic Research Institute, Kolkata 700032, India*
[b]*Non-Oxide Ceramics and Composite Division, CSIR-Central Glass and Ceramic Research Institute, Kolkata 700032, India*

Received 7 September 2012; accepted 9 September 2012
Available online 23 September 2012

Abstract

Hydroxyapatite (HAp)-based highly porous integrated orbital implants with a property of mimicking the movements of fellow eye have been developed recently. Before designing this kind of scaffolds, vascularization and angiogenesis in the constructs need to be considered. Moreover, eye cells expressed with time on these highly porous implants may exert some compressive load whose effect both mechanically and physiologically may indicate its long-term life in vivo. In the present investigation the effect of expression of eye cell lines [rabbit corneal epithelial cell line (SIRC)] on highly porous HAp scaffolds were compared with the normal fibroblastic cells on HAp in general, in terms of in vitro dissolution studies, cell culture cytotoxicity and cell adhesion properties. Elastic properties of macro-porous HAp with a wide range of porosities have also been estimated by ultrasonic non-destructive test methods and the results were compared with its compressive properties for potential application as integrated ocular implants. Cell viability of HAp in contact with SIRC is far better than the L-929 during the initial periods (48 h) but cell adhesion behavior however showed better results in L-929 than the SIRC during the same initial time period. SIRC cells however eventually formed better adhesion properties on the surface of HAp as the days goes by than L-929. High concentration of both Ca and P in culture media might be another factor in cell growth modification. Both the ions had a counter effect on the L-929 and SIRC cells.

Keywords: Macro-porous Hydroxyapatite; Elastic properties; Rabbit corneal epithelial cell line (SIRC); Integrated ocular implants

1. Introduction

Porous hydroxyapatite (HAp), a major constituent of mammalian bone, has found a wide variety of applications, e.g., for cell loading, as drug releasing agent, in chromatography analysis and, most extensively, as hard tissue scaffolds. Recently HAp based highly porous integrated orbital implants with a property of mimicking the movements of fellow eye have also been developed [1,2]. Before designing this kind of scaffolds of HAp, vascularization and angiogenesis in the constructs need to be considered [3]. Pore interconnections provide the channel for cell distribution and migration allowing efficient in vivo blood vessel formation. Vascularization, besides providing nutrients essential for tissue survival, plays a crucial role in coordinating the activity of cells and their migration for new tissue formation. This entire mass thus produced in situ in vivo may exert some pressure on the ocular implants. Another factor which could be very important is the intraocular pressure. The average normal intraocular pressure is about 15 mm Hg with a range from 12–20 mm Hg (i.e. ~0.0016–0.0027 MPa) [4]. Eye cells thus expressed with time on these highly porous implants may exert some compressive load whose effect both mechanically and physiologically may indicate its long-term life in vivo. To the best of our knowledge, effect of eye cell lines on these highly porous HAp implants is unknown. Rabbit corneal epithelial cell line (SIRC) has been extensively utilized in a

*Corresponding author. Tel.: +91 9831772081; fax: +91 33 24730957.
E-mail address: biswa_kundu@rediffmail.com (B. Kundu).
[†]Deceased on 10 May 2012.

0272-8842/$ - see front matter © 2012 Elsevier Ltd and Techna Group S.r.l. All rights reserved.
http://dx.doi.org/10.1016/j.ceramint.2012.09.031

wide range of investigations, including studies in which the corneal cells serve as indicators for predicting the ocular toxicity and irritancy potential of various compounds [5,6]. Although not sated as such, the implication of such studies is that the SIRC cell might serve as an in vitro correlate for at least a portion of the corneal surface.

A correlation is also known to exist between the dissoluted ions (mainly Ca^{2+} and PO_4^{3-}) from HAp in contact with physiological fluid in vivo and this eye cell expression with time. HAp is also well-known for its non-toxicity, biocompatibility, non-immunogenicity in contact with different osteoblasts and fibroblastic cells both in vitro and in vivo. But, said parameters have not been studied in case of eye cells. Porous HAp implants are also frequently used as osteo-conductive bone scaffolds whose final applications are limited to non-load bearing region of human body. The sintered density and microstructure of the final sintered HAp control the mechanical properties of the scaffolds. Optimization of sintering properties and judicious controlling of microstructure are known to enhance the strength and toughness of HAp products [7]. In spite of its importance in designing biomedical components, elastic properties of porous HAp have not been studied extensively. These studies are limited to fairly low porosity levels (30%–45%) or dense varieties [8–11]. However, this property is very important to understand materials' interaction with mineralized tissues and subsequent calcified tissue behavior after implantation.

In this paper, we have tried to address the issues like (1) effect of expression of eye cell lines on the highly porous HAp scaffolds which was compared with the normal fibroblastic cells on HAp in general, in terms of in vitro dissolution studies, cell culture cytotoxicity and cell adhesion properties and for the first time (2) elastic properties of macro-porous HAp with wide range of porosities which have been estimated using ultrasonic NDT (non-destructive testing). The results of porous struts were also compared with its compressive properties suitable for ocular implant applications.

2. Experimental

2.1. Synthesis

HAp powder was synthesized in the laboratory by a wet chemical method using analytical reagent grade calcium hydroxide and ortho-phosphoric acid as the initial reactants with the Ca/P molar ratio of these two reactants maintained at ~1.67. Details of the procedures along with details of powder characterization could be found elsewhere [1,12,13]. Powders calcined at 800 °C were used for fabrication of porous scaffolds samples while 1250 °C was selected as the sintering temperature. As for the fabrication of porous bodies, the powder calcined at 800 °C was intimately mixed with appropriate quantity of naphthalene (SD Fine-Chem, India) powder by repeated sieving in a sieve shaker (Retsch, AS200, Germany). Porous units were fabricated by modification of a process developed earlier [1]. In the present investigation, naphthalene was added in different percentages for scaffold formulation, viz., 10%–70%, (hereinafter the same designated as P1, P2, P3, P4 and P5). The powder mix was subsequently compacted at a pressure of 150 MPa (for 40 s) by cold-isostatic pressing (EPSI N.V.; SO 10036, Belgium) to form cylindrical shaped green specimens. Specimens having required dimensions suitable for further characterization were machined using a manual lathe machine. By heating up to 80 °C, the naphthalene was driven off from the green specimens with care to prevent cracking, at this stage. Finally, the green and now fragile specimens were sintered at 1250 °C for 2 h (heating rate 30 °C/min. and air atmosphere).

2.2. Microstructural characterization

Physical properties including apparent or open porosity and bulk density of the sintered porous specimens were measured by Archimedes' principle (ASTM astm:C373-88) [14]. Microstructure, pore size, shape and morphology were observed by field emission scanning electron microscopy (FESEM) (Carl Zeiss, Supra 35 VP, Germany) on one side of the flat-parallel surface while transmission electron microscopy (TEM) (Tecnai G2 30, FEI, Netherlands) was used for powder characterization when fired at 1250 °C. Image analysis was carried out to calculate the pore size distribution (Perfect Screen Ruler 2.0, Styopkin Software, USA). More than 250 linear measurements were taken from each micrograph and converted to their actual dimension from the corresponding tag of each microstructure. Histograms thus obtained were plotted as function of pore size ranges. The average pore sizes were also determined. The microstructures were mainly taken in the back-scatter electron mode. Samples were mounted and sputter-coated (Polaron, Quoram Technology, U.K.) with gold-palladium having a coating thickness ~6 nm to reduce charging and to improve the image quality prior testing.

2.3. Estimation of mechanical properties

Compressive strength tests were performed in triplicate for each kind of samples series. Sample dimensions for the compressive strength measurement was selected as per the ASTM specification [15], i.e., for cylindrical specimens the length:diameter ratio was 2:1. Elastic properties of the sintered specimens at wide range of porosities were estimated primarily by ultrasonic NDT, supported by destructive mechanical testing.

An Instron Universal Testing Machine (5500R) was used to determine the ultimate compressive strength of the sintered HAp ceramics destructively. The cross-head speed was 0.5 mm/min. Opposite faces of all samples were made flat and parallel using a diamond grinding wheel prior the tests. On the other hand, elastic moduli (Young's modulus, E and shear modulus, G) and Poisson's ratio (v) of porous, sintered specimens were estimated non-destructively using ultrasonic wave velocities. Cylindrical specimens of 12.5 mm nominal

diameter and thickness in the range of 2.1–2.3 mm were prepared with varying average porosities. The sintered samples were subjected to lapping and polishing to render the two opposite ends of circular cross sections flat and parallel. The HAp specimens with varying porosities were assumed to be isotropic [9,10]. However, unlike previous researchers [8,10] who reported moduli values for HAp samples for low to moderate range of porosities, i.e., up to 32%–45% porosity only, the present work has been carried out for estimation of elastic moduli spanning a larger range of porosities from 10% to 65% which has not been reported hitherto by any other researchers. The longitudinal and transverse ultrasonic waves (L-wave and S-wave) were launched by an Olympus EPOCH 4 Plus ultrasonic flaw detector from one end of the sample and received at the opposite end by means of a pair of 2.25 MHz Panametric make L-wave and S-wave ultrasonic transducers, respectively. From the respective time domain ultrasonic signals, the time of flight in microseconds and the sample thickness in mm were used to obtain the ultrasonic L-wave and S-wave velocities, V_L and V_S, respectively using standard relations [16]. The porosity (p), the elastic moduli (E and G) and the Poisson's ratio (v) of the samples were obtained as follows:

$$p = 1 - \frac{\rho}{\rho_0} \tag{1}$$

$$G = \rho V_S^2 \tag{2}$$

$$E = \rho V_S^2 \frac{(3V_L^2 - 4V_S^2)}{(V_L^2 - V_S^2)} \tag{3}$$

In Eq. (1), ρ_0 refers to the theoretical density of hydroxyapatite. The magnitude of ρ_0 is taken as 3.156 g/cm^3. The Poisson's ratio is determined from the well known relation between E and G as follows:

$$v = 1 - \frac{E}{2G} \tag{4}$$

2.4. Bioactivity studies

To study the dissolution behavior and in vitro bioactivity of the porous specimens suitable for ocular implant application, dissolution tests were conducted in triplicate in SBF (simulated body fluid). The SBF was prepared according to Kokubo formulation [17]. Assays were performed by immersing each porous specimen in 30 mL of SBF solutions using 50 mL capacity polypropylene flasks, thermostatized (37 ± 0.5 °C) and statically kept up to different time intervals at that temperature. The experiment was conducted according to ISO 10993-14 [18]. After immersion periods of 1, 4, 7 and 14 days and after decanting the supernatant, the samples were kept for further microscopic observation and the collected solution were centrifuged at 4000 rpm for 5 min in DDW (double distilled water) and subsequently analyzed for different cations and anions. ICP-AES (inductively coupled plasma-atomic emission spectra; STM 08, Spectro-Analytical Instruments, Germany) was used to determine the calcium and phosphorus concentration in the supernatants. Chemical and physical changes, occurred after immersion in the physiological saline in different time intervals, if any, were observed by SEM-EDAX (scanning electron microscopy-energy dispersive analysis of X rays; LEOS 430i, UK with Lithium drifted Silicon detector for EDAX) on the sample surface. Depending on the samples composition, microstructures were taken either in secondary electron or back-scatter electron mode. The samples were sputter-coated prior to testing with carbon having a coating thickness ~5–20 nm to reduce the electron charging effect.

Cell viability assays were performed by the following protocols. Rabbit corneal epithelial cell line (SIRC) [National Centre for Cell Science (NCCS), Pune, India) were first cultured at 37 °C in a humidified atmosphere at 5% CO_2 in air, in 10 cm Petri dish containing 10 mL of DMEM [Dulbecco's modified Eagles Medium (Gibco)] supplemented with 10% fetal calf serum, 100 U/mL Penicillin (Sigma), 50 μg/mL streptomycin (Sigma) and 50 μg/mL and gentamycin (Sigma). When the cells were grown up to 80%–90% of cellular confluence, the cultured cells were differentiated with trypsin-EDTA. The porous HAp substrates were autoclaved (120 °C, 20 min), placed in 6-well plate (70 mm diameter) and desired volume of DMEM was added (0.2 g of the substrates weight—1 mL of DMEM was added). The plate was incubated at (37 ± 2) °C for 24 h, and the extracted medium was collected. Then previously differentiated cells were collected and diluted in DMEM medium. The cells were counted using hemocytometer. 2×10^3 cells were suspended in extracted medium was plated in the 96-well plate (1 cm^2) in triplicates for each substrate and incubated at (37 ± 2) °C for 48 and 96 h with positive control as glass cover slip. After incubation for the above periods, MTT reagent [3-(4,5-dimethylthiazole-2-yl)-2,5-phenyltetrazolium bromide] was added and incubated for 4 h at 37 °C to deoxidize MTT. The reaction was stopped by adding acidified isopropanol. The absorbance was measured at 490 nm in an ELISA reader, the percentage of cell viability for individual substrates were obtained. Similar procedures were followed when L-929 mouse fibroblast cells were used to check the cell viability in contact with the dense HAp.

Cell adhesion behavior was studied in the present investigation by using the SIRC cell line. As before, SIRC cells were seeded on porous HAp surface and glass cover slip at density of 2×10^3 cells/cm^2 and incubated for 48 h at (37 ± 2) °C under humidified atmosphere containing 5% CO_2. Cell seeded porous HAp and glass cover slips were fixed in 2.5% glutaraldehyde and processed by dehydrating in graded ethanol. Samples were then subjected to critical point drying followed by Au-sputtering. Cell seeded porous HAp and control cover slip was examined under an SEM. Similar procedures were followed when L-929 mouse fibroblast cells were used to check the cell adhesion behavior in contact with the dense HAp.

3. Results and discussion

Details of HAp powder characterization can be found elsewhere [1,12,13]. Very briefly, XRD of the powders prepared at 80 °C and calcined at 800 and 1250 °C were well matched with the standards in JCPDS PDF (Joint Committee on Powder Diffraction Standards Powder Diffraction Files) no. 09-0432 which corresponds to the phase pure HAp. Polycrystalline nature and purity of the phase were retained up to 1250 °C. Powders calcined at 800 °C were used to fabricate the porous blocks. Percent crystallinity which is the direct evidence of the amorphous content in the fabricated materials, increased from 67.6% to 98.3% when the powders were fired at 800–1250 °C. FTIR band assignments showed respective functional groups for PO_4^{3-} and OH^- corresponding to HAp crystals. Band positions of OH^- at 3580 and 630 cm^{-1} were absent in case of as-prepared powders fired at 800 °C. A small hump at the wave number 1454 cm^{-1} was also found and corresponded to vibrations of CO_3^{2-} ions. This effect was found to be more pronounced in powders calcined at 800 °C. At 1250 °C, however, carbonate peaks became insignificant. The bands at 1454 and 1414 cm^{-1} attributed to CO_3^{2-} groups in the apatite structure are evident [19,20]. The band at 865 cm^{-1} was assigned to both types of incorporation. At 1250 °C, the intensity of the bands both at 1454 and 1414 cm^{-1} were decreased. This could be interpreted as a release of carbonate from PO_4^{3-} positions in the apatite structure.

Physical parameters such as percent open or apparent porosity (AP), bulk density (BD) of different porous HAp scaffolds measured by Archimedes' water displacement method are given in Table 1. It was found that the open porosity was increasing with the amount of added naphthalene followed by concomitant decrease in bulk density. There was sharp increment of porosity only when the naphthalene quantity was added more than 30% to the mixture with 800 °C calcined powders. Ideally, this % AP should be directly related with the naphthalene % added to the green body fabrication. But this is not the case in the present investigation as revealed from the microstructure observed. All samples were studied for microstructure with the pore size, shape and distribution using FESEM. Photomicrographs obtained have been reported in Fig. 1A–E as function of % naphthalene added to the green body. Further, every micrograph was analyzed to calculate the pore size distribution. Histograms thus obtained were plotted and represented in Fig. 2A–E. All the statistical plots were shown as a function of increment of naphthalene added to the green body.

It was found from Fig. 1A–E that both micron to nano-sized pores were present in all the microstructures. With increasing amount of naphthalene the spherical nature of pore shape started to change. This means that release of naphthalene during drying of the green body, was more uniform through the major matrix of HAp (P1 and P2 samples, Fig. 2A and B) than the condition at lower amount of HAp matrix. This observation was more prominent from P3 samples (Fig. 2C–E). With the amount of naphthalene increase, these void shapes become ruptured and more and more non-uniform release of the fugitive material occurred. The microstructure reported in Fig. 2C–E thus, were found to be more non-uniform. However, adequate interconnection of pores was observed for all microstructures. Usually these types of additive particles volatilize leaving isolated porosity, consisting of spherical voids connected by narrow necks [21]. Fig. 1A–E show this distribution of pores in the matrix when naphthalene quantity was increasing from 10% to 60%. P2 samples showed more numbers of nano-pores than any other samples. It was observed that amount of nano-pores started increasing from P1 samples to P2 samples although naphthalene addition was increased by ~10%. Amount of micropores, however, was found to increase when naphthalene addition was increasing from 40% to 50%. P4 sample was composed of almost equal distribution of micro- and macropores. Above 50% of naphthalene added, macropores were found to be predominant and this trend continued up to 60% naphthalene addition. Average pore sizes were calculated and are reported in Table 1. Both the values were similar for all the samples except P2 samples, where most of the pores fell within micron to nano-sized pores. Significance of these pore sizes are already explained earlier. Most of the images of FESEM were taken in the back-scatter mode. BSE imaging provides a quick and convenient method of examining the distribution of chemistry within a material and qualitatively separating region of high and low atomic numbers. Porous regions, where there is no material, provided good contrast. It is well reported now that FESEM images are analyzed with various computer software to measure porosity and pore sizes [22] and for statistical analysis, different sample sizes are used, for

Table 1
Variation of different physical properties with addition of pore formers and average and median pore sizes calculated from Fig. 1.

Sample	A.P. (%)	Average pore size (μm)	B.D. (g/cm^3)	Pore size range (μm)	Median pore size (μm)
P1	4.99	69.8	2.67	0.97–286	40.8
P2	10.19	55.4	2.39	0.6–351	2.4
P3	43.38	91.7	1.74	14–335	69.9
P4	54.19	114.3	1.47	15–399	92.3
P5	64.29	140.2	1.11	26–469	125.5

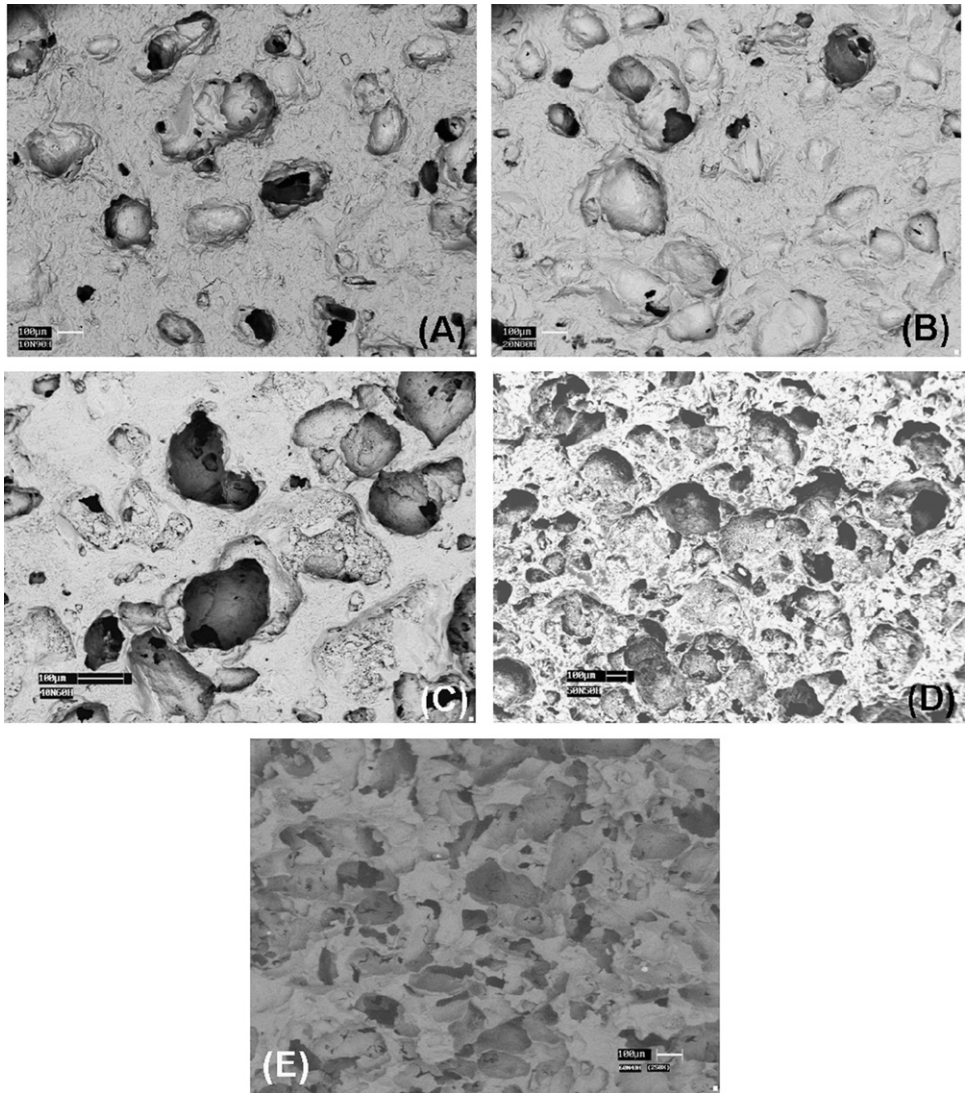

Fig. 1. SEM microstructure of samples (A) P1, (B) P2, (C) P3, (D) P4 and (E) P5.

example, ranging from measures from 10 to 40 pores to a minimum of 100 [23]. In the present study, on an average 250 pores were measured from particular micrographs and the said statistical graphs were plotted (Fig. 2A–E). Degree of pore connectivity is dependent on bulk density and degree of isotropy of the specimen. So, it is practically difficult to accurately identify structural relationships. Some trends could be evident, however, between variation of macropore size and morphology and BD. As expected, mean macropore sizes were found to increase with decreasing BD. Pore connectivity was found to be influenced by both macrostructural anisotropy and BD, with the influence of BD on connectivity being stronger for isotropic specimens, particularly for specimens with higher BD. This observation also corroborates the findings of Hing et al. [24]. However, micropores were found to be independent of specimen BD with increasing quantity of naphthalene addition. From the FESEM microstructure it was also evident that microporosity could be divided into two groups depending on the size. Nanopores (< 1 μm in size) tended to be isolated spherical pores, which were randomly distributed throughout the ceramic struts, more predominantly in P1 and P2 specimens, most probably located at grain boundaries, triple points and occasionally positioned within grain (please refer Fig. 1A and B as well as the TEM micrograph of Fig. 3 for the powders fired at 1250 °C). Micropores with size range from 1 to 25 μm appeared to be interconnected too (like the macropores), with irregularity in shape and orientation, with respect to their neighbors, within the porous struts. However, the evolution of the pore network is difficult to analyze quantitatively. Rhines and De Hoff [25] deduced that the evolution of the pore network contains features that were comparable to those of other topological decay processes such as grain growth in fully dense polycrystalline solids.

As volatiles are removed from the green body, empty pore space is created. The binder-vapor interfaces shown to penetrate toward the interior of the green body in either a planar or non-planar front represents a boundary between diffusion of volatiles in the organic phase and in the gaseous

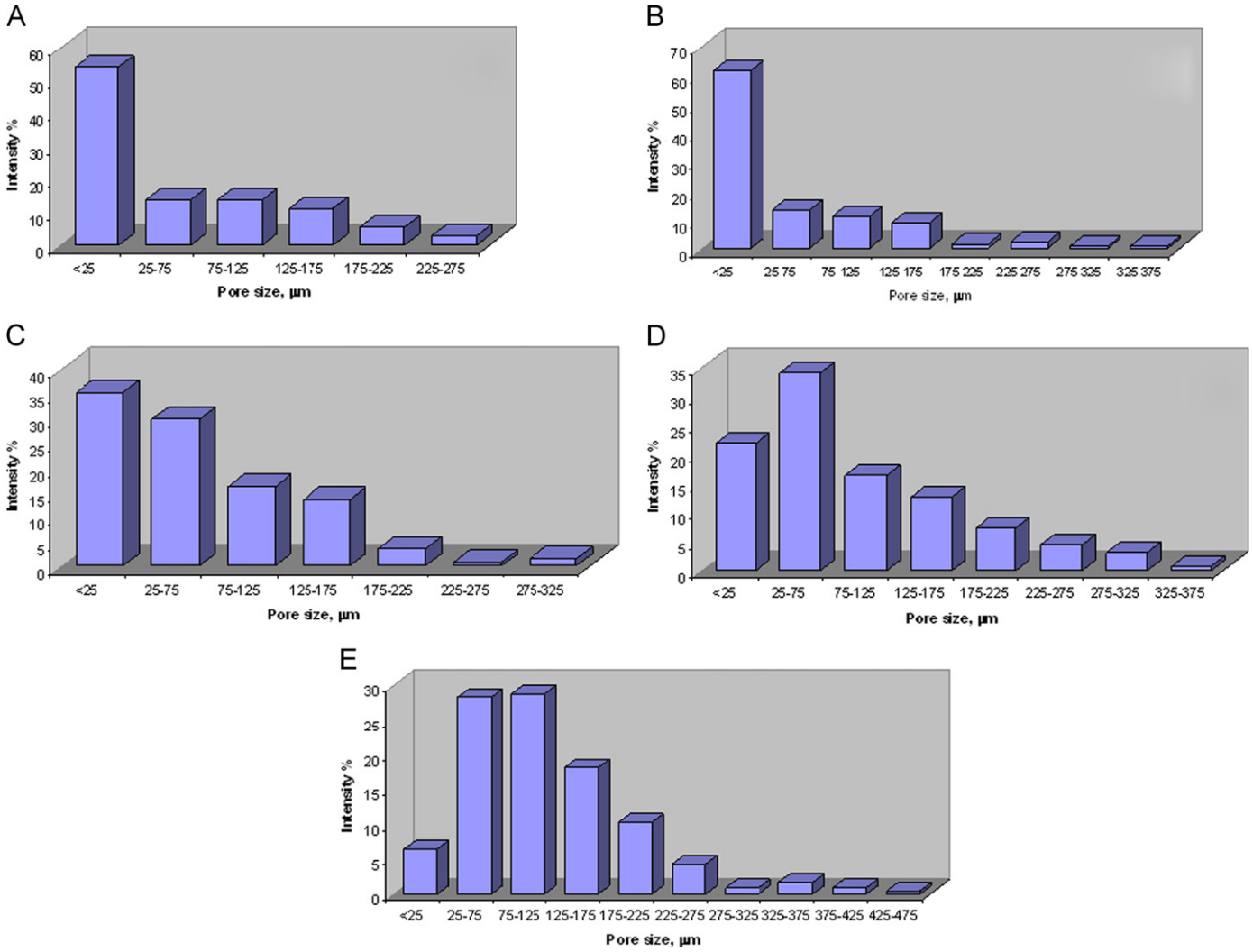

Fig. 2. Histogram showing the pore size distribution of (A) P1, (B) P2, (C) P3, (D) P4 and (E) P5 samples.

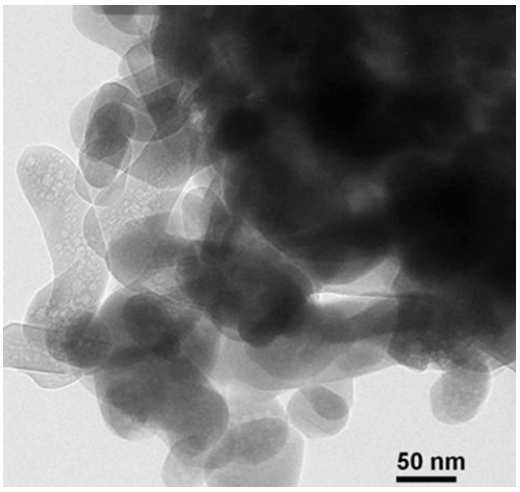

Fig. 3. Bright-field TEM image of HAp powders fired at 1250 °C.

phase (i.e., empty pores). Because of differences in volatile diffusivities between these two phases, the processes by which binders distribute within the green body during thermolysis are intimately coupled to their removal kinetics [26]. Naphthalene was not intimately bound to the powder. As a result, its removal generated non-planar interface. Since the HAp powder had some amorphous content (as obtained from XRD of powders calcined at 800 °C), after generation of this interface, the samples actually gave nice particle–particle contact in the green body. Amorphous content acted like binder for the green samples devoid of naphthalene. FESEM microstructures of P4 and P5 samples showed very non-uniform with high interconnectivity of pores. A bimodal distribution of pores was seen for P5 samples. Macropores >50 μm) were mainly evidenced from both the micrographs and with lesser amount of micropores in P5 samples than the P4 one. The average pore size for both these kinds of samples were calculated and found to be $\sim$114.3 and 140.2 μm for P4 and P5 samples respectively. It was noticed that with increasing amount of naphthalene, the spherical nature of pore shapes (when the naphthalene percentage was only $\sim$5%–10%) started to change and the void shapes were ruptured (when the naphthalene percentage was $\sim$30%). More and more non-uniform release of this fugitive

material was evident and so the microstructures of P4 and P5 samples. However, superior interconnection of pores was found for all micrographs. Sub-surface interconnections were found in the range from 30–120 μm throughout the microstructures of P5 samples and about 10–100 μm for P4 samples.

Compressive investigations [27,28] into a numbers of key test-piece parameters, such as specimens' shape, aspect ratio and size, have demonstrated that cylindrical specimens with an aspect ratio of 2:1 (length:diameter) should be standardized for compression testing of high porosity materials. Gibson [29] successfully predicted mechanical properties of highly porous ceramics with about 6%–90% porosity by modeling the structure as an elastic brittle foam. The relationships derived were of the following form:

$$\sigma_c \infty c_a \cdot \rho^x \tag{5}$$

where σ_c is the compressive stress, c_a is the constant, ρ is the bulk density and x is the geometrical parameter that depends on both isotropic nature of the porous specimen as well as the direction of testing with respect to the pore texture. De Groot et al. [30] on the other hand showed the dependence of σ_c on total pore volume (V_p) for calcium phosphate ceramics and gave the following relationships:

$$\sigma_c = 700\exp(-5V_p) \tag{6}$$

where V_p is in the range of 0–0.5. For the present case, σ_c as function of calculated open porosity percentage as well as bulk density is given in Fig. 4.

It was found that there was sharp fall of the value of σ_c when porosity increased from ~2.2% to 5% and subsequently it followed an exponential decaying up to ~75% porosity. A second order exponential decay relationships having the following form, has been successfully fitted:

$$y = A_1 e^{-c_1 x} + A_2 e^{-c_2 x} \tag{7}$$

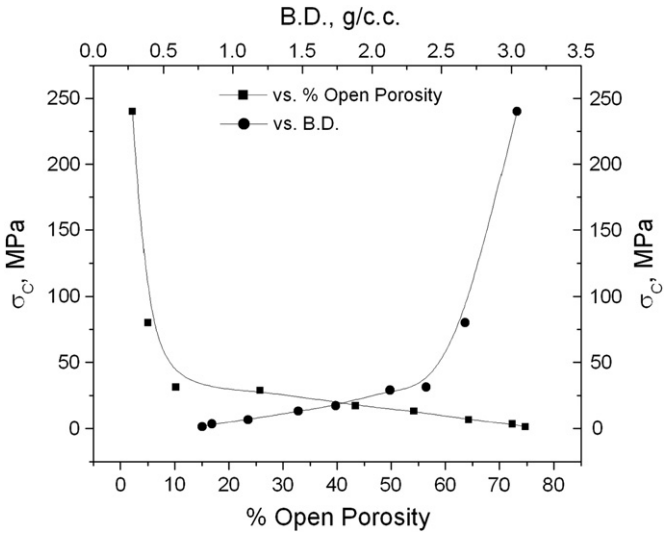

Fig. 4. Variation of compressive strength of the porous bodies fabricated using different percentage of naphthalene with percentage open porosity and bulk density.

where y is the ultimate compressive strength, A_1 and A_2 are the amplitudes, c_1 and c_2 are the decay constants and x is the corresponding open porosity percent. Statistically, χ^2 and R^2 were found to be ~23.25 and 0.998 respectively. Corresponding bulk density values were also used as another parameter and σ_c as a function of these BD values were found to be matched with a kind of exponential growth having the following generic form:

$$y = Ae^{cx} \tag{8}$$

where y is the ultimate compressive strength, A and c are amplitude and growth constant respectively, x is the corresponding bulk density value. Statistically, χ^2 and R^2 were found to be ~64.02 and 0.990 respectively.

Microstructural anisotropy did not have any particular effect on the values of σ_c. Rather it was strongly dependent on the open pore volume as well as the corresponding apparent density values. In the present study, pore geometry was not varied and hence its effect on σ_c could not be inferred. As expected, the median pore sizes decreased with increasing bulk density (Table 1), but it was the total percentage of open pore which affected the decreased values of σ_c with decreasing BD. For example, P2 samples had much higher micropores than the other samples having a median pore size of only ~2.4 μm. Even then it showed decreasing tendency of σ_c with the total open pore percent. With increasing amount of naphthalene and as seen from pore size distribution evidence (cf. Fig. 2), P3 samples' micropores amount started decreasing and macropores started increasing while P4 samples onwards it was mainly the macropores which played the role to give the σ_c values nearly linear and closer with increment of percentage of open porosity. Now, it has been widely accepted that an ideal tissue-engineered bone substitute should be a synthetic scaffold, which is biocompatible and provides for cell attachment, proliferation and maturation, has mechanical properties to match those of the tissue at the site of implantation and degrades at rates to match tissue replacement. Scaffold may not be necessarily required to provide complete mechanical equivalence to a healthy tissue, but stiffness and strength should be sufficient to at least support and transmit forces to the host tissue site in the context. For example, in skin tissue engineering, the construct should be able to withstand the wound contraction forces. From the results of compressive strength values and owing to the above facts, it could be inferred that for present application in ocular environment, P5 samples having an average σ_c value ~6.6 MPa could be selected. This value is also very close to the compressive strength value of cancellous bone [31].

Elastic modulii of porous HAp, namely, the Young's modulus (E) and shear modulus (G) have been estimated from ultrasonic longitudinal and shear wave velocities for a very wide range of higher percentage of porosities, which has not been reported so far in literature. In the low porosity range, both the longitudinal and shear wave velocities could be ascertained from the ultrasonic time domain signals which exhibited sharp distinct peaks for first and second backwall echoes. Ultrasonic longitudinal

wave signals were detected with better clarity compared to the shear wave velocities, with a dominant peak even at larger levels of porosity. Due to extreme fragility of highly porous HAp specimens, estimation of shear wave velocities was considerably difficult. To circumvent this problem, a novel methodology was developed for estimation of shear modulus from ultrasonic longitudinal wave velocity only [32]. The elastic moduli E and G were calculated with the help of Eqs. (3) and (4). The estimated values of Young's modulus and shear modulus versus porosity are plotted in Fig. 5.

The variation of elastic moduli of porous HAp with porosity followed a general trend typical of porous, brittle ceramics as reported by previous researchers [33,34]. In the present work, the values of zero porosity elastic modulii for phase pure hydroxyapatite were taken from Gilmore and Katz [35] as $E_0=114$ GPa and $G_0=45$ GPa, respectively. For porous, brittle ceramics, the variation of elastic moduli with porosity has been fitted with many different expressions as reported by Phani and Niyogi [33]. In the present work also, the experimental variation of elastic moduli (E and G) with porosity for phase pure HAp samples synthesized using the wet chemical route has been attempted with the help of a semi-empirical expression:

$$M = M_O\left(1-p/p_c\right)^{n_M} \tag{9}$$

where M is the elastic modulus (E or G), p_c is the critical porosity at which the elastic modulus becomes zero and n_M (i.e, n_E or n_G) is the pore structure dependent parameter for the modulus M (E or G). Eq. (9) was fitted to the experimental data for E versus p and G versus p variations, as shown in Fig. 5, with the E_0 and G_0 values as reported above, yielding $p_c=0.95$ and $n_E=n_G=2.33$. The fit between the data and correlation was evaluated with the help of the sum of squares Q defined in terms of the mean and the theoretically estimated modulus values, $\overline{S}$ and $\hat{S}_i$, respectively, as follows:

$$Q = 1-\frac{\sum_{i=1}^{n}(S_i-\hat{S}_i)^2}{\sum_{i=1}^{n}(S_i-\overline{S})^2} \tag{10}$$

A value of $Q=0.97$ indicates a very good fit between the two. From Fig. 5, it is clearly observed that the porous HAp body looses 92% of its stiffness at 65% porosity compared to that of the pore free body. Clearly there ought to be a trade off between the increased level of tissue growth and decreased elastic stiffness with increasing level of porosity while designing a HAp based scaffold.

Apart from mechanical behavior, the issue of bioactivity of the porous HAp was also analyzed methodically. According to Kokubo and Takadama [17], a bioactive material is a material on which bone-like hydroxyapatite will form selectively after it is immersed in a serum-like solution. Dissolution study was performed following some modification of the process from the literature on this. 1 × SBF was used throughout the process, test was performed at $p(CO_2)\sim 1$ atmospheric pressure, no agitation was given while these were kept for dissolution at pH 7.4 and temperature of 37.4 °C. From the crystallization theory, thermochemical calculations show that serum and SBF are supersaturated toward apatite crystals [36] and the bioactivity test was performed in a plastic container with smooth surface and without scratches because apatite nucleation can be induced at the surface of a glass container or the edge of scratches. 6 × SBF or 1 × SBF with pH 6.0 was not at all used to perform the study since composition and physiological condition would not be the same respectively. That is why Ca^{2+} or PO_4^{3-} ion concentration was determined for this blank 1 × SBF kept for 0, 3 and 7 days respectively. These values were deducted from the dissolute SBF's (into which samples were kept individually for 1, 4, 7 and 14 days) Ca^{2+} and PO_4^{3-} ion concentration. Samples' weight gain/loss for the study period was also recorded. The weight profile and the Ca^{2+} and PO_4^{3-} ion concentration of the supernatant solution were given in Fig. 6A and B respectively as function of the days of study.

The weight profiles were obtained after normalizing the individual sample's weight prior immersion in SBF. It was found from Fig. 6A that there was a net weight loss up to 4th day, after which there were many-fold net weight gain up to 14th day. Similarly, there was maximum net dissolution of Ca^{2+} and PO_4^{3-} up to 4th day. The dissolution rate after that day decreased drastically and continued up to 14th day. According to Kokubo and Takadama [17], bioactive compound is a material that accelerates heterogeneous apatite crystallization in a solution supersaturated towards hydroxyapatite. This can be achieved by several strategies: (a) providing apatite nuclei that remove the need to nucleate apatite crystals, (b) providing a surface with a low interfacial energy with apatite or (c) changing the local supersaturation towards apatite precipitation. In the present case the first strategy was predominating and corroborated the findings of Kim et al. [22] and Juhasz et al. [37]. Probably dissolution and

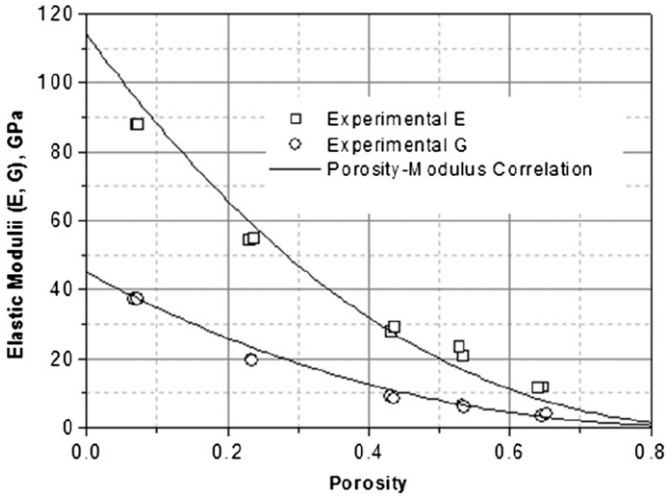

Fig. 5. Variation of elastic modulii (E and G) of porous HAp estimated ultrasonically with different porosity levels.

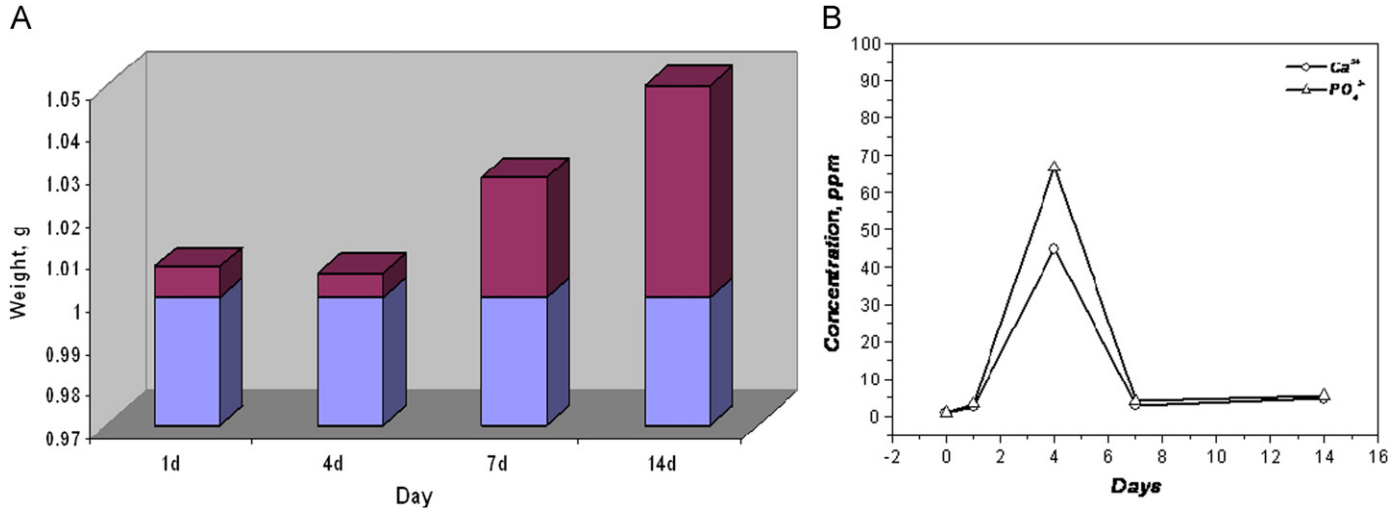

Fig. 6. In vitro dissolution studies: (A) weight profile of porous HAp and (B) concentration of the eluting solution after different days of immersion in 1× SBF.

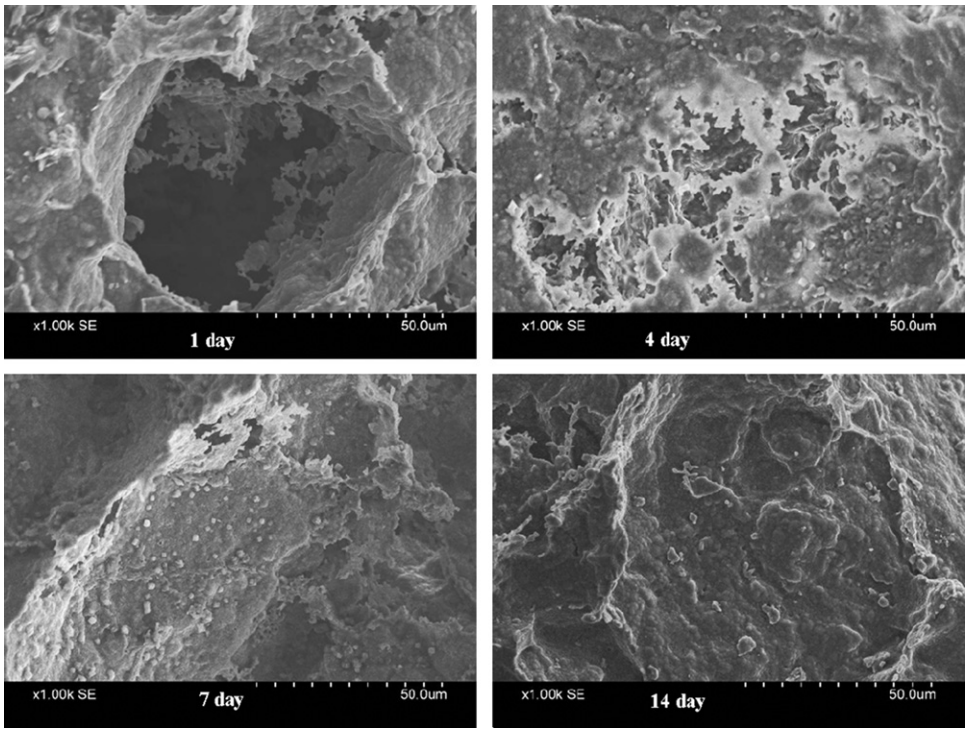

Fig. 7. SEM microstructures of sample taken after soaking in 1× SBF at pH 7.4 and temperature of 37.4 °C at different time interval (under different magnifications).

precipitation was occurring in contact with the SBF solution. Throughout the study period, it was the equilibrium of these two phenomena. It could be seen from Fig. 6B that, both PO_4^{3-} and Ca^{2+} dissolution started from day 1 and reached a maximum on day 4, thereafter there was still dissolution occurring, but from Fig. 6A, it could be understood that dissolution–precipitation balance moved and the precipitation was the main phenomena occurring after day 4. Every analysis of supernatant SBF, however, there was more PO_4^{3-} ion than the corresponding Ca^{2+}. The possible explanation will be discussed as follows with respect to the microstructure observed obtained after soaking in SBF at different time interval. These are given in Figs. 7 and 8.

On day 4, there were two types of phenomena occurring as revealed from the microstructure. There was both formation of cavity as well as deposition of petal-like morphology and cubic crystal (Fig. 8) which could be due to the formation HAp and $CaCO_3$ on the surface respectively. Both the phenomena (dissolution–precipitation) were occurring by day 4. Most probably it was the formation of bone-like apatite (petal-like morphology), $Ca_{10-x}(PO_4)_{6-x}(CO_3)_x(OH)_2$ in which, a part of PO_4^{3-} was substituted by CO_3^{2-}. At this

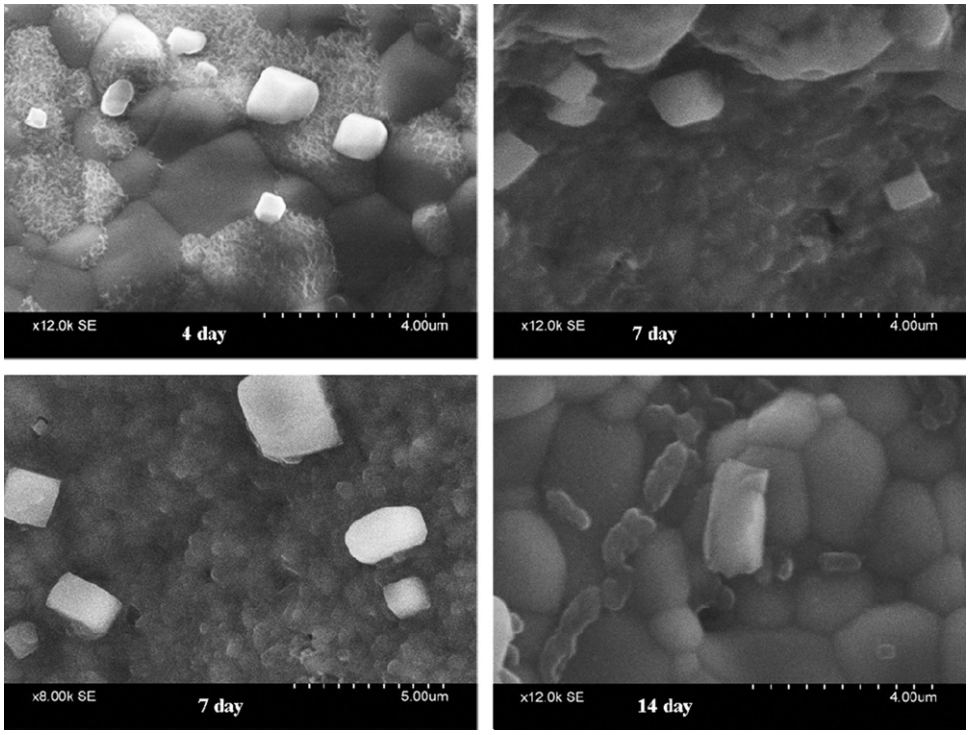

Fig. 8. SEM microstructures of sample taken after soaking in 1 × SBF at pH 7.4 and temperature of 37.4 °C at different time interval (under different magnifications).

point, large numbers of nucleation sites formed on the surface. The nucleation and growth at these nucleation sites consumed a lot of Ca^{2+} and PO_4^{3-} in SBF. The calcium and phosphate ion consumptions exceeded the supply by dissolution and resulted in the decrease in both the ion concentration after 4th day. Therefore, it was considered that the deposition of petal-like crystals of HAp occurred by the reaction between Ca^{2+} and PO_4^{3-} ions both from dissolved HAp or by the reaction between Ca^{2+} from porous HAp and phosphate ions (PO_4^{3-}, HPO_4^{2-}, $H_2PO_4^{-}$) from the SBF. The amorphous HAp formed on the surface became crystallized and formed small-carbonate containing HAp crystals. Precipitation rate was slower after 7 days due to lack of necessary ions, such as Ca^{2+} and PO_4^{3-}, for the formation of apatite in the solution. High percentage of porosity with >50 μm interconnection facilitated faster dissolution of the samples than the corresponding samples with lower percentage of porosity in contact with SBF. There were many sites of nucleation on the porous scaffold and nuclei could not grow much larger in a limited ion source [38].

The SIRC cell line has been extensively utilized in a wide range of investigations, including studies in which the corneal cells serve as indicators for predicting the ocular toxicity and irritancy potential of various compounds. Although not sated as such, the implication of such studies is that the SIRC cell might serve as an in vitro correlate for at least a portion of the corneal surface [5,6]. On the other hand, ISO 10993 part 5, 1999 prefers the use of established cell lines such as L-929, Balb/3T3 and WI-38 for cytotoxicity testing. These cell lines provide good reproducibility for in vitro cytotoxicity screening owing to their homogeneous morphology and growth characteristics. The L-929 cell line is a mouse fibroblast cell. A detailed literature search shows that L-929 cells are being widely used for cytotoxicity analysis [39]. Hence we have also selected these cells for in vitro cytotoxicity evaluation of both dense and porous HAp. SIRC Cellular response around the porous HAp as viewed microscopically is given in Fig. 9A. On cytotoxicity scale the score was '0', which as par ISO specification was completely non-cytotoxic. Healthy cells could be noticed from the photomicrograph. Characteristic spindle-shaped SIRC cells containing an elongated nucleus and long cytoplasmic processes (morphologic characteristics reminiscent of corneal keratocytes) could be seen. Negative control (UHMWPE in this case) gave non-cytotoxic response and positive control (PVC) gave severely cytotoxic responses as expected. Similar results were also observed when L-929 mouse fibroblasts were used as culture. Using L-929 and with both the methods (direct contact and test on extract) of ISO 10993 part 5, 1999, it was found that both dense and porous HAp showed much healthier and grown up cells on top of each surfaces compared to the positive control, where clear cell destruction could be found. Moreover, the cells were grown uniformly on the dense body compared to porous samples due to less surface area available for spreading of the cells. Direct contact is recommended for low density materials, such as contact lens polymers. During incubation, any leachable chemicals from the test material can diffuse into the culture medium and contact directly with the cell layer. The chemicals released are concluded to be cytotoxic if malformation, degeneration and lysis of cells are observed around the test

material. This was not the case for both dense and porous HAp.

Ocular implants has direct contact with both the eye epithelial tissues and it is expected that with due course of time, leachables like Ca^{2+} and/or PO_4^{3-} may come out from the HAp based implants. This is the reason why both direct contact and extraction cytotoxicity were checked. In the present observation good correlation however found between direct and indirect contact tests. A good cell-material contact method would replicate more closely the physiological situation in vivo which in turn would give more clinically relevant results [40].

Cell viability is a determination of living or dead cells, based on a total cell sample in contact with the said material of interest. Cell viability measurements assess healthy cells in a sample. This can be accomplished either by directly counting the number of healthy cells or by measuring an indicator for healthy cells in cell populations (e.g., in a microplate assay). Whether the cells are actively dividing or quiescent is not distinguished. An increase in cell viability indicates cell growth, while a decrease in viability can be interpreted as the result of either toxic effects of compounds/agents or suboptimal culture conditions. Most viability assays are based on one of two characteristic parameters: metabolic activity or cell membrane integrity of healthy cells. Usually the metabolic activity is measured in cell populations via incubation with a tetrazolium salt (e.g., MTT, XTT, WST-1) that is cleaved into a colored formazan product by metabolically active cells.

The cytotoxicity/cell viability of the porous hydroxyapatite was assessed by the MTT cytotoxicity assay. MTT assay of adhered SIRC cells were performed at the end of 48 and 96 h. The cells on test sample showed 122% and 358% metabolic activity after the same period respectively compared to the activity of control coverslip at 48 h. It was 100% metabolic activity when the dense HAp was used to study the cell viability MTT assay after 48 h. By analyzing the results obtained, it can be observed that the hydroxyapatite scaffolds are biocompatible and that the cells adhere and proliferate well when compared to the control.

In Fig. 9, it may be seen in detail, the cell adhesion and morphology of the hydroxyapatite in day 2 of cell culture of SIRC. On the second day of cell culture, the cells started spreading over the available surface of HAp scaffold. Cells' philopodia were strongly attached to several points of the grains as it can be observed in Fig. 9B. Control cover slip showed a better cellular adhesion and spreading compared to porous HAp on day 2 (Fig. 9C). In contrast, L-929 cells were covered more to the surface of HAp with strongly attached philopodia to much higher numbers of grains after day 2 (Fig. 9D). Morphologies of L-929 cells in contact with control cover slip are given in Fig. 6E for comparison purpose.

Two things were observed from these data: (1) cell viability of HAp in contact with SIRC is far better than the L-929 during the initial periods (48 h), (2) cell adhesion behavior however showed better results in L-929 than the SIRC during the same time period. There are many factors which may contribute, e.g., surface charge, wettability on the initial anchoring of the cells to ceramics [41] etc. It was also found that the wettability of the ceramic career was related to the ionic density within the thin surface layer [42]. In addition, the surface structure of HAp/tri-calcium phosphate (TCP) ceramics was observed to be altered by the association and dissociation of calcium and phosphate in the tissue culture medium [43]. Surface instability of implant material is considered to cause inflammation of the surrounding tissues due to the high reactivity at the cell-material interface. In fact, a lag phase in cell growth of one day is often observed in vitro for osteoblast and fibroblast cells on synthesized HAp and composite materials [44]. High concentration of both Ca and P in culture media might be another factor in cell growth modification [45]. It could be seen that both these elements were leaching faster after 2 days in contact with SBF. So, it could be said that these ions also increased in the culture media which gave the dissolution/reprecipitation process occurring at the surface of the material evolved throughout the culture period [45]. Both the ions had a counter effect on the L-929 and SIRC cells. On one hand, more and more viable cells of SIRC came in contact with the surface of HAp in presence of Ca and P in culture media; on the other hand, lesser viable L-929 cells came into contact during the same period. Since all other parameters including zeta potential, surface wettability were constant, it is the behavioral differences of the cells in contact with Ca and P of culture media which showed contrasting results. The physicochemical events occurring at the interface between calcium phosphate materials are thought to be responsible for the chemical bonding of bioactive implants with bone. LeGeros et al. summarized these events as follows [46]:

(1) Decrease in the pH in the environment of the calcium phosphate ceramics causing partial dissolution of the ceramic macrocrystal;
(2) Increase in the concentration of calcium and phosphate ions in the micro-environment;
(3) Formation of CO^{3-} apatite crystals (by precipitation, by transformation from one Ca–P phase to another, or by seeded growth) incorporating ions (e.g., carbonate, magnesium) from the biological fluids [47];
(4) Association of the CO^{3-} apatite microcrystals with an organic matrix; and
(5) Incorporation of these microcrystals with the collagenous matrix during the formation of new bone at the interface. Based on this process, the balance of ions between stages (1), (2), and (3) would be related directly to the surface of the ceramic grains.

SIRC cells eventually formed better adhesion properties on the surface of HAp as the days goes by than L-929, which showed a better anchorage in the initial periods (as more

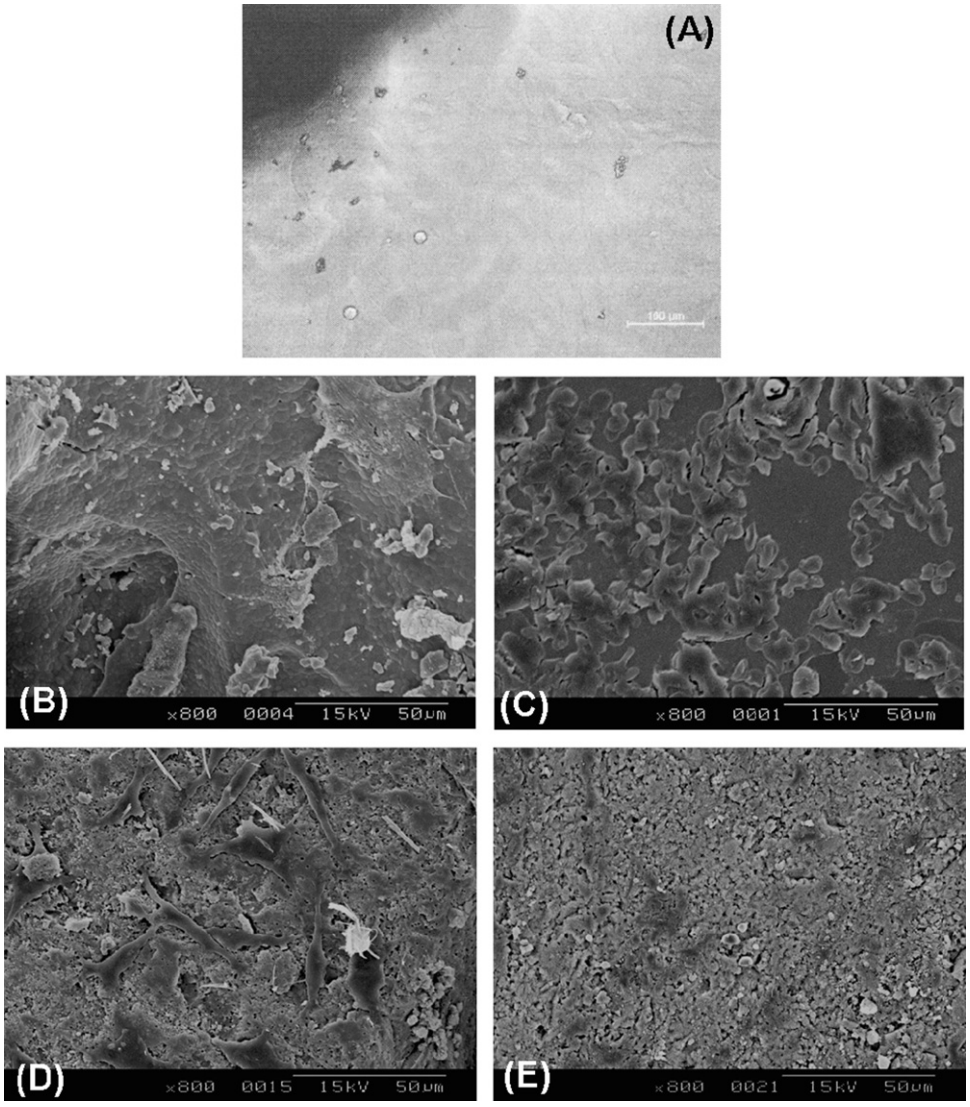

Fig. 9. SIRC cells around porous HAp sample (A), SEM morphology of SIRC cells in contact with porous HAp sample (B) and control (glass cover slip) (C) after 48 h (both under $\times 800$ magnification), SEM morphology of L-929 mouse fibroblast cells in contact with porous HAp sample (D) and control (glass cover slip) (E) after 48 h (both under $\times 800$ magnification).

philopodia or microspikes were observed in this case). Microspikes are slender cytoplasmic projections, similar to lamellipodia, which extend from the leading edge of migrating cells [48]. They contain actin filaments cross-linked into bundles by actin-binding proteins, e.g., fimbrin [49]. Philopodia form focal adhesions with the substratum, linking it to the cell surface. A cell migrates along a surface by extending philopodia at the leading edge. This attach to the substratum further down the migratory pathway, then contraction of stress fibers retracts the rear of the cell to move the cell forwards.

4. Conclusions

Estimation of elastic moduli for porous bioceramic scaffold material made of synthetic hydroxyapatite has been carried out using ultrasonic NDT. The elastic properties have been evaluated for a much wider range of porosities which have not been reported by other researchers so far. A semi-empirical modulus versus porosity correlation has been developed for porous HAp which shows excellent match with experimentally measured data. For present application in ocular environment, P5 samples having an average σ_c value of $\sim$6.6 MPa could be selected. This value also very close to the compressive strength value of cancellous bone. Cell viability of HAp in contact with SIRC is far better than the L-929 during the initial periods (48 h) but cell adhesion behavior however showed better results in L-929 than the SIRC during the same initial time period. SIRC cells eventually formed better adhesion properties on the surface of HAp as the days goes by than L-929. Surface instability of implant material is considered to cause inflammation of the surrounding tissues due to the high reactivity at the cell-material interface. In fact, a lag phase in cell growth of one day is observed in vitro for osteoblast and fibroblast cells on synthesized HAp and

composite materials. High concentration of both Ca and P in culture media might be another factor in cell growth modification. It could be seen that both these elements were leaching faster after 2 days in contact with SBF. So, it could be said that these ions were also increased in the culture media which made the dissolution/reprecipitation process occur at the surface of the material evolve throughout the culture period. Both the ions had a counter effect on the L-929 and SIRC cells. On one hand more and more viable cells of SIRC came in contact with the surface of HAp in presence of Ca and P in culture media, on the other hand, less viable L-929 cells came into contact during the same period.

Acknowledgments

The authors wish to express their sincere thanks the Director, CSIR-CGCRI, India for his generous and kind support to this work. Assistance from all personnel related to the characterization (like SEM, FESEM, TEM, ICP-AES, etc.) of the materials is sincerely acknowledged. Thanks are also due to the Scientists of Sree Chitra Tirunal Institute for Medical Sciences and Technology (SCTIMST), Trivandrum, India for carrying out some of the cellular studies at their end. The authors would also like to thank Indo-US Forum for Science and Technology (IUSSTF) for their support in carrying out some of the investigations.

References

[1] B. Kundu, M.K. Sinha, M.K. Mitra, D. Basu, Fabrication and characterization of porous hydroxyapatite ocular implant followed by an in vivo study in dogs, Bulletin of Materials Science 27 (2) (2004) 133–140.

[2] T.P. Colen, D.A. Paridaens, H.G. Lemij, M.P. Mourits, W.A. van Den Bosch, Comparison of artificial eye amplitudes with acrylic and hydroxyapatite spherical enucleation implants, Ophthalmology 107 (10) (2000) 1889–1894.

[3] S. Sedrakyan, Z.Y. Zhou, L. Perin, K. Leach, D. Mooney, T.H. Kim, Tissue engineering of a small hand phalanx with a porously casted polylactic acid-polyglycolic acid copolymer, Tissue Engineering 12 (9) (2006) 2675–2683.

[4] A.C. Guyton, J.E. Hall, The eye: I. Optics of vision, in: A.C. Guyton, J.E. Hall (Eds.), Textbook of Medical Physiology, Elsevier Saunders, Pennsylvania, 2006, p. 624.

[5] C. Korbmacher, H. Helbig, C. Forster, M. Wiederholt, Characterization of Na^+/H^+ exchange in a rabbit corneal epithelial cell line (SIRC), Biochimica et Biophysica Acta 943 (3) (1988) 405–410.

[6] J.Y. Niederkorn, J.S. Peeler, J. Mellon, Phagocytosis of particulate antigens by corneal epithelial cells stimulates interleukin-1 secretion and migration of Langerhans cells into the central cornea, Regional Immunology 2 (2) (1989) 83–90.

[7] M.A. Fanovitch, J.M. Porto Lopez, Influence of temperature and additives on the microstructure and sintering behaviour of hydroxyapatites with different Ca/P ratios, Journal of Materials Science: Materials in Medicine 9 (1) (1998) 53–60.

[8] D.S. Metsger, M.R. Rieger, D.W. Foreman, Mechanical properties of sintered hydroxyapatite and tricalcium phosphate ceramic, Journal of Materials Science: Materials in Medicine 10 (1) (1999) 9–17.

[9] O. Prokopiev, I. Sevostianov, J. Genin, S.M. McGee, C. Woodward, Microstructure and elastic properties of sintered hydroxyapatite, International Journal of Fracture 130 (3) (2004) L183–L190.

[10] O. Prokopiev, I. Sevostianov, Dependence of the mechanical properties of sintered hydroxyapatite on the sintering temperature, Materials Science and Engineering: A 431 (1–2) (2006) 218–227.

[11] W.Y. Ching, P. Rulis, A. Misra, Ab initio elastic properties and tensile strength of crystalline hydroxyapatite, Acta Biomaterialia 5 (8) (2009) 3067–3075.

[12] B. Kundu, A. Lemos, C. Soundrapandian, P.S. Sen, S. Datta, J.M.F. Ferreira, D. Basu, Development of porous HAp and β-TCP scaffolds by starch consolidation with foaming method and drug-chitosan bilayered scaffold based drug delivery system, Journal of Materials Science: Materials in Medicine 21 (11) (2010) 2955–2969.

[13] B. Kundu, C. Soundrapandian, S.K. Nandi, P. Mukherjee, N. Dandapat, S. Roy, B.K. Datta, T.K. Mandal, D. Basu, R.N. Bhattacharya, Development of new localized drug delivery system based on ceftriaxone-sulbactam composite drug impregnated porous hydroxyapatite: a systematic approach for in vitro and in vivo animal trial, Pharmaceutical Research 27 (8) (2010) 1659–1676.

[14] C373-88, Standard Test Method for Water Absorption, Bulk Density, Apparent Porosity, and Apparent Specific Gravity of Fired Whiteware Products, American Standard for Testing and Methods, ASTM, 2006.

[15] C773-88, Standard Test Method for Compressive (Crushing) Strength of Fired Whiteware Materials, American Standard for Testing and Methods, ASTM, 2006.

[16] J.X. Lu, B. Flautre, K. Anselme, P. Hardouin, A. Gallur, M. Descamps, B. Thierry, Role of interconnections in porous bioceramics on bone recolonization in vitro and in vivo, Journal of Materials Science Materials in Medicine 10 (2) (1999) 111–120.

[17] T. Kokubo, H. Takadama, How useful is SBF in predicting in vivo bone bioactivity?, Biomaterials 27 (15) (2006) 2907–2915.

[18] 10993-14:2001, Biological Evaluation of Medical Devices—Part 14: Identification and Quantification of Degradation Products From Ceramics, International Organization for Standardization, ISO, 2001.

[19] T.S.B. Narasaraju, D.E. Phebe, Some physico-chemical aspects of hydroxylapatite, Journal of Materials Science 31 (1) (1996) 1–21.

[20] Y. Suetsugu, I. Shimoya, J. Tanaka, Configuration of carbonate ions in apatite structure determined by polarized infrared spectroscopy, Journal of the American Ceramic Society 81 (3) (1998) 746–748.

[21] D. Shi, Bioceramic processing, in: Introduction to Biomaterials, Tsinghua University Press, Beijing, China, 2006, p. 31.

[22] H.M. Kim, T. Himeno, M. Kawashita, T. Kokubo, T. Nakamura, The mechanism of biomineralization of bone-like apatite on synthetic hydroxyapatite: an in vitro assessment, Journal of the Royal Society, Interface 1 (1) (2004) 17–22.

[23] J.J. Barry, H.S. Gidda, C.A. Scotchford, S.M. Howdle, Porous methacrylate scaffolds: supercritical fluid fabrication and in vitro chondrocyte responses, Biomaterials 25 (17) (2004) 3559–3568.

[24] K.A. Hing, S.M. Best, K.E. Tanner, W. Bonfield, P.A. Revell, Quantification of bone ingrowth within bone-derived porous hydroxyapatite implants of varying density, Journal of Materials Science Materials in Medicine 10 (10/11) (1999) 663–670.

[25] E.N. Rhines, R.T. De Hoff, Sintering and heterogeneous catalysis, in: G.C. Kuczynski, A.E. Miller, G.A. Sargent (Eds.), Materials Science Research, vol. 16, Plenum, New York, 1984, pp. 49–61.

[26] J.A. Lewis, Binder removal from ceramics, Annual Reviews of Materials Science 27 (1997) 147–173.

[27] F. Linde, I. Hvid, F. Madsen, The effect of specimen geometry on the mechanical behaviour of trabecular bone specimens, Journal of Biomechanics 25 (4) (1992) 359–368.

[28] T.M. Keaveny, R.E. Borchers, L.J. Gibson, W.C. Hayes, Trabecular bone modulus and strength can depend on specimen geometry, Journal of Biomechanics 26 (8) (1993) 991–1000.

[29] L.J. Gibson, M.F. Ashby, in: Cellular Solids: Structure and Properties, 2nd ed., Cambridge University Press, Cambridge, UK, 1997.

[30] K. De Groot, C.P.A.T. Klein, J.G.C. Wolke, J. De Blieck-Hogervorst, Chemistry of calcium phosphate bioceramics, in: T. Yamamuro, L.L. Hench, J. Wilson (Eds.), Handbook of Bioactive Ceramics, vol. 2, CRC Press, Boca Raton, FL, 1990, pp. 3–15.

[31] M. Jarcho, Calcium phosphate ceramics as hard tissue prosthetics, Clinical Orthopaedics and Related Research 157 (1981) 259–278.
[32] D. Sanyal, B. Kundu, D. Basu, Estimation of elastic properties of porous, sintered bioceramic scaffold material using ultrasonic NDT, in: Proceedings of the National Seminar and Exhibition on Non-Destructive Evaluation (NDE 2011), Chennai Trade Centre, Chennai, India, 2011.
[33] K.K. Phani, S.K. Niyogi, Elastic modulus porosity relation in polycrystalline rare-earth oxides, Journal of the American Ceramic Society 70 (11) (1987) C362–C366.
[34] K.K. Phani, D. Sanyal, The relations between the shear modulus, the bulk modulus and Young's modulus for porous isotropic ceramic materials, Materials Science and Engineering: A 490 (1–2) (2008) 305–312.
[35] R.S. Gilmore, J.L. Katz, Elastic properties of apatites, Journal of Materials Science 17 (4) (1982) 1131–1141.
[36] X. Lu, Y. Leng, Theoretical analysis of calcium phosphate precipitation in simulated body fluid, Biomaterials 26 (10) (2005) 1097–1108.
[37] J.A. Juhasz, S.M. Best, A.D. Auffret, W. Bonfield, Biological control of apatite growth in simulated body fluid and human blood serum, Journal of Materials Science Materials in Medicine 19 (4) (2008) 1823–1829.
[38] J.W. Cahn, On the morphological stability of growing crystals, in: H.S. Peiser (Ed.), Crystal Growth, Pergamon Press, Oxford, 1967, p. 681.
[39] T.Y. Saw, T. Cao, A.U. Yap, M.M. Lee Ng, Tooth slice organ culture and established cell line culture models for cytotoxicity assessment of dental materials, Toxicology In Vitro 19 (1) (2005) 145–154.
[40] T. Cao, T.Y. Saw, B.C. Heng, H. Liu, A.U. Yap, M.L. Ng, Comparison of different test models for the assessment of cytotoxicity of composite resins, Journal of Applied Toxicology: JAT 25 (2) (2005) 101–108.
[41] K. Nishizawa, M. Toriyama, T. Suzuki, Y. Kawamoto, Y. Yokogawa, H. Nagae, Effects of the surface wettability and zeta potential of bioceramics on the adhesiveness of anchorage-dependent animal cells, Journal of Fermentation and Bioengineering 75 (6) (1993) 435–437.
[42] M. Toriyama, Y. Kawamoto, T. Suzuki, Y. Yokogawa, K. Nishizawa, F. Nagata, Wettability of calcium phosphate ceramics by water, Journal of the Ceramic Society of Japan 103 (1995) 46–49.
[43] T. Suzuki, T. Yamamoto, M. Toriyama, K. Nishizawa, Y. Yokogawa, M.R. Mucalo, Y. Kawamoto, F. Nagata, T. Kameyama, Surface instability of calcium phosphate ceramics in tissue culture medium and the effect on adhesion and growth of anchorage-dependent animal cells, Journal of Biomedical Materials Research 34 (4) (1997) 507–517.
[44] D.A. Puleo, L.A. Holleran, R.H. Doremus, R. Bizios, Osteoblast responses to orthopedic implant materials in vitro, Journal of Biomedical Materials Research 25 (6) (1991) 711–723.
[45] P. Frayssinet, N. Rouquet, J. Fages, M. Durand, P.O. Vidalain, G. Bonel, The influence of sintering temperature on the proliferation of fibroblastic cells in contact with HA-bioceramics, Journal of Biomedical Materials Research 35 (3) (1997) 337–347.
[46] R.Z. LeGeros, Calcium phosphates in oral biology and medicine, in: H.M. Mayers (Ed.), Monographs in Oral Science, vol. 15, Karger, New York, 1991, p. 32.
[47] M. Heughebaert, R.Z. LeGeros, M. Gineste, A. Guilhem, G. Bonel, Physicochemical characterization of deposits associated with HA ceramics implanted in nonosseous sites, Journal of Biomedical Materials Research 22 (3 Suppl) (1988) 257–268.
[48] P.K. Mattila, P. Lappalainen, Filopodia: molecular architecture and cellular functions, Nature Reviews 9 (6) (2008) 446–454.
[49] D. Hanein, P. Matsudaira, D.J. DeRosier, Evidence for a conformational change in actin induced by fimbrin (N375) binding, The Journal of Cell Biology 139 (2) (1997) 387–396.